Chinese Chemical Letters 36 (2025) 109720

Contents lists available at ScienceDirect

Chinese Chemical Letters

journal homepage: www.elsevier.com/locate/cclet

Metal-organic framework Cu-BTC for overall water splitting: A density functional theory study

Xu Huang[a], Kai-Yin Wu[a], Chao Su[a], Lei Yang[b,*], Bei-Bei Xiao[a,*]

[a] School of Energy and Power Engineering, Jiangsu University of Science and Technology, Zhenjiang 212003, China
[b] School of Chemistry and Chemical Engineering, Institute for Computation in Molecular and Materials Science, Nanjing University of Science and Technology, Nanjing 210094, China

ARTICLE INFO

Article history:
Received 24 January 2024
Revised 19 February 2024
Accepted 1 March 2024
Available online 6 March 2024

Keywords:
Metal-organic framework
Density functional theory
Cu-BTC
Photocatalysis
Overall water splitting

ABSTRACT

Metal-organic framework (MOF) has been widely applied in photocatalysis, which is significant for addressing energy crises and environmental issues. Based on density functional theory calculations, the performances of Cu-BTC, a copper-based MOF, and its derivatives CuTM-BTC *via* the substitution of transition metal (TM) elements at the Cu site for photocatalytic overall water splitting (POWS) have been studied. POWS of Cu-BTC suffers from the sluggish hydrogen evolution reaction due to the large overpotential of 2.02 V and limited solar utilization due to a wide HOMO-LUMO gap of 4.11 eV. *Via* TM substitution, the HOMO-LUMO gap narrows but still satisfies the redox potentials when taken 3d-TM of Cr, Fe, Co or Ni, 4d-TM of Rh or Pd, or 5d-TM of Re or Pt into consideration, benefiting for the light absorption. Furthermore, Cr and Re could serve as active sites for hydrogen evolution with remarkably lowered overpotentials of 0.79 V and 0.28 V, respectively; similarly, oxygen evolution activities could be enhanced by Fe, Co and Rh because of their reduced overpotentials which are less than 0.5 V. Therefore, our findings pave guidance for designing Cu-BTC derivatives in overall water splitting.

© 2025 Published by Elsevier B.V. on behalf of Chinese Chemical Society and Institute of Materia Medica, Chinese Academy of Medical Sciences.

The excessive consumption of conventional fossil fuels and the accompanying environmental issues have prompted humanity to eagerly develop alternative energy conversion technologies [1–3], among which photocatalysis has been regarded as one of the most prospective candidates. Through the utilization of appropriate photocatalysts, photocatalytic technology converts solar energy into chemical energy. Photocatalytic overall water splitting (POWS), a promising technology of large-scale hydrogen and oxygen production from sunlight in an environmentally friendly manner without renewable resources utilization and carbon dioxide emission, has attracted tremendous attention [4–6].

The phenomenon of POWS was first discovered by Japanese scientists Fujishima and Honda in 1972 [7], who found the generation of hydrogen gas and oxygen gas during the illumination experiment on TiO_2 electrodes. POWS reaction, comprising two half-reactions: hydrogen evolution reaction (HER) and oxygen evolution reaction (OER), generally occurs in three steps [8–10]. First of all, when photocatalytic semiconductor materials are radiated by incident light with energy greater than their band gap, the electrons in the valence band of semiconductor materials will be excited and transfer to the conduction band, leaving holes in the valence band. Subsequently, electrons and holes gather in the conduction band and valence band respectively, generating photoexcited electron-hole pairs. And then, photoexcited carriers separate and migrate to the surface of semiconductor through diffusion, during which the recombination of photoexcited carriers will cause competitive effects. Eventually, the photoexcited carriers which successfully migrate to the semiconductor surface undergo redox reaction with adsorbed species on the surface to generate hydrogen and oxygen. The efficiency of the first two steps of the reaction mainly depends on the performance of the photocatalyst material itself, such as the electronic band structure, and the edge alignment of the band [11,12], while the third step which is promoted by cocatalysts is the committed step to determine the rate of POWS, because of the slow kinetics of redox on the catalyst surface [9]. These harsh conditions pose a huge challenge for designing efficient photocatalysts. Hence, in recent years, great efforts have been made to explore highly-efficient and robust photocatalysts to boost the efficiency of POWS. Varieties of semiconductor photocatalytic materials, including metal oxides [13–15], sulfides [16–18], nitrides [19–21], and nonmetal materials [22–24], are utilized in the research of POWS. In addition, modification strategies such as cocatalyst loading [13,25–27] and heterojunction engineering [28–30] have been proposed to diminish the band

* Corresponding authors.
E-mail addresses: yanglei21@njust.edu.cn (L. Yang), xbb420@just.edu.cn (B.-B. Xiao).

https://doi.org/10.1016/j.cclet.2024.109720
1001-8417/© 2025 Published by Elsevier B.V. on behalf of Chinese Chemical Society and Institute of Materia Medica, Chinese Academy of Medical Sciences.

gap of semiconductor materials and improve their visible light response, which have been verified through experimental and theoretical studies. For example, owing to the unique electronic structure and excellent chemical stability, g-C_3N_4 is widely used for photocatalytic decomposition of water [24,31,32]. Nonetheless, the rapid recombination of photoexcited carriers leads to its low photocatalytic activity. Ding *et al.* found that the light absorption range of g-C_3N_4 expands, and the recombination of photoexcited carriers also decreases with the incorporation of transition metal cations such as Fe^{3+}, Co^{3+}, Ni^{3+} and Cu^{2+} [11,32–34]. Through density functional theory (DFT) calculations, Wang and coworkers discovered that *via* introducing MoS_2 which inherently has a lower band gap into g-C_3N_4, the formed heterojunction narrows the band gap, enhances light absorption and also decreases the recombination of photoexcited carriers [35]. Although modification methods have been adopted to achieve efficient POWS under visible light irradiation, most of them need the assistance of cocatalysts. In the sense, it is imperative to explore a photocatalyst and a cocatalyst in harmony.

Metal-organic frameworks (MOFs), composed of metal ions or clusters and organic ligands, are a class of porous crystal materials with periodic network structure [36–39], which is a hot topic in material science and has been widely applied in different fields such as catalytic conversion [39,40], gas adsorption and separation [41,42], energy storage battery [43,44], and biomedicine [38,45] due to its advantages of uniform pore volume, large specific surface area, flexible and adjustable structure, and excellent thermal stability. First reported by Chui *et al.* in 1999 [46], Cu-BTC, a typical copper-based MOF with tetrahedral side pockets, large square-shaped channels and cuboctahedral cages, is composed of dimeric cupric tetracarboxylate units. Cu-BTC has been widely used in the field of catalysis due to the presence of highly dispersed unsaturated metal sites in its skeleton structure that can act as catalytic active sites. For instance, Schelichte *et al.* found that Cu-BTC can selectively catalyze the cyanosilane reaction of benzaldehyde and trimethylsilyl cyanide [47], achieving 57% yield, which was far higher than the yield of other catalysts. Additionally, Cu-BTC composite materials or derived materials also have good catalytic performances. Dong *et al.* designed a W-Cu-BTC *via* substituting a Cu atom in Cu-BTC and predicted it as a potential candidate catalyst for CO_2 hydrogenation to formic acid [48], whose energy barrier was 0.30 eV The research results of Jin *et al.* indicated that CuO@Cu-BTC composite possessed distinguished methylene blue degradation activity under visible light [49], whose degradation efficiency (98%) outclassed the pristine CuO (75%) and Cu-BTC (80%), and it also showed good photocatalytic HER activity. As one of the most paradigmatic photocatalytic materials, there are still few reports focused on Cu-BTC for POWS, as its wide band gap (>3 eV) brings the inherent shortage of its poor visible light response ability [50].

In this text, based on DFT calculations, a systematic study was conducted on POWS performances of Cu-BTC and its derivates CuTM-BTC which was constructed *via* the substitution of transition metal elements at the Cu site. The results reveal that Cu-BTC is relative inert due to poor light response and low HER activity. *Via* element substitution, the structural feasibility of CuTM-BTC was evaluated by considering substitution energy E_{diff}. Then, the HOMO and LUMO orbitals distributions in combination with absorption spectra were checked to reveal the response toward light utilization. Afterward, the free energy profiles were analyzed to assess the HER/OER overpotentials. Finally, the thermodynamic feasibility of a photo-redox reaction was assessed by comparing HER overpotentials η^{HER} and OER overpotentials η^{OER} with the LUMO-reduction offset (LRO) and HOMO-oxidation offset (HOO), respectively. According to our results, Cr or Re can serve as an HER active site and Fe, Co or Rh can serve as an OER active site. This study provides guidance to optimizing CuTM-BTC in the POWS application.

According to the previous reports [48,51], the Cu-containing cluster models are cut from the unit of Cu-BTC in order to simplify the calculations (Fig. 1a). Consisting of one Cu-Cu paddle-wheel unit along with four benzene-1,3,5-tricarboxylate (BTC) organic linkers, the Cu-BTC cluster model comprises 58 atoms, including 28 C atoms, 8 O atoms, and 2 Cu atoms. In addition, the carboxyl group on the benzene ring is substituted by H atoms to predigest the configuration, so the number of H atoms in the cluster reaches 20. This simplified model can rationally mimic the unsaturated metal sites of the Cu-BTC, which is also regarded as the active sites involved in photocatalysis, and it has been employed in erstwhile works, such as methanol adsorption and CO oxidation [52,53]. One of the Cu atoms in this cluster model is subsequently replaced by several transition-metal elements to achieve better reaction performance (Fig. 1b), and the new cluster is abbreviated as CuTM-BTC. 26 transition metal elements shown in Fig. 1b are considered, excluding Tc, Cd, La, and Hg due to their toxicity.

For Cu-BTC cluster, each Cu atom connecting four carboxylic O atoms and the other Cu atom, are unsaturated and defined as the photocatalytic active site. After TM substitution, CuTM-BTCs still maintain a stable and symmetrical structure, being consistent with the previous results [54,55]. In the following discussion, we mainly focus our attention on the photocatalytic performance of TM site without considering the Cu site. The computational methods are given in Supporting information.

After geometric optimization, the maximum bond length $d_{TM\text{-}O(max)}$ and minimum bond length $d_{TM\text{-}O(min)}$ between the TM and O atoms of CuTM-BTC are collected and listed in Table 1. Quantitatively, the deviation degree ε of the metal atoms was adopted to evaluate the deviation of TM atoms in CuTM-BTC [56], which is defined as $\varepsilon = (1 - d_{TM\text{-}O(min)}/d_{TM\text{-}O(max)}) \times 100\%$. With exception of CuV-BTC, all ε are less than 0.2%, suggesting that there is almost no deviation of TM atoms from the center of CuTM-BTC, which reflects that CuTM-BTC has a good symmetry characteristic. Furthermore, to estimate the structural feasibility, the substitution energy E_{diff} of CuTM-BTC relative to Cu-BTC is given in Fig. 2. With exception of Zn, Ag, and Au, E_{diff} of CuTM-BTC are negative, indicating that the TM substitution at the Cu site is energetic-feasible. Herein, due to its unstable characteristic, CuZn-BTC, CuAg-BTC and CuAu-BTC are not taken into consideration in the following discussions.

The excellent POWS photocatalyst should have an appropriate band gap, which is conducive to light absorption. Meanwhile, it should also have appropriate redox potential to drive the half-reactions [11,57,58]. HER requires that the conduction band minimum (CBM) or the lowest unoccupied molecular orbital (LUMO) of the photocatalyst is higher than the reduction potential of H^+/H_2 (−4.44 eV at pH 0), while OER requires that the valence band maximum (VBM) or the highest occupied molecular orbital (HOMO) is lower than the oxidation potential of H_2O/O_2 (−5.67 eV at pH 0) [59,60]. In order to investigate the photoexcitation, HOMO-LUMO orbital alignments to the redox reactions are calculated. Table S1 (Supporting information) lists the energy levels of the frontier orbitals evaluated *via* different functionals, PBE *vs.* B3LYP. Wherein, it is clear that the PBE functional severely underestimates the energy gap, which is much smaller than those calculated by B3LYP functional. It is in line with previous literatures [61–63]. In the regard, B3LYP functional was adopted to calculate the photoelectric properties herein.

As shown in Fig. 3a, Cu-BTC has a large HOMO-LUMO gap with the value of 4.11 eV, reflecting its poor response to visible light and thereby limiting its photocatalytic application, which is consistent with previous report [50]. When 3d-TM of Cr, Fe, Co or Ni, 4d-TM of Rh or Pd, 5d-TM of Re or Pt is considered as sub-

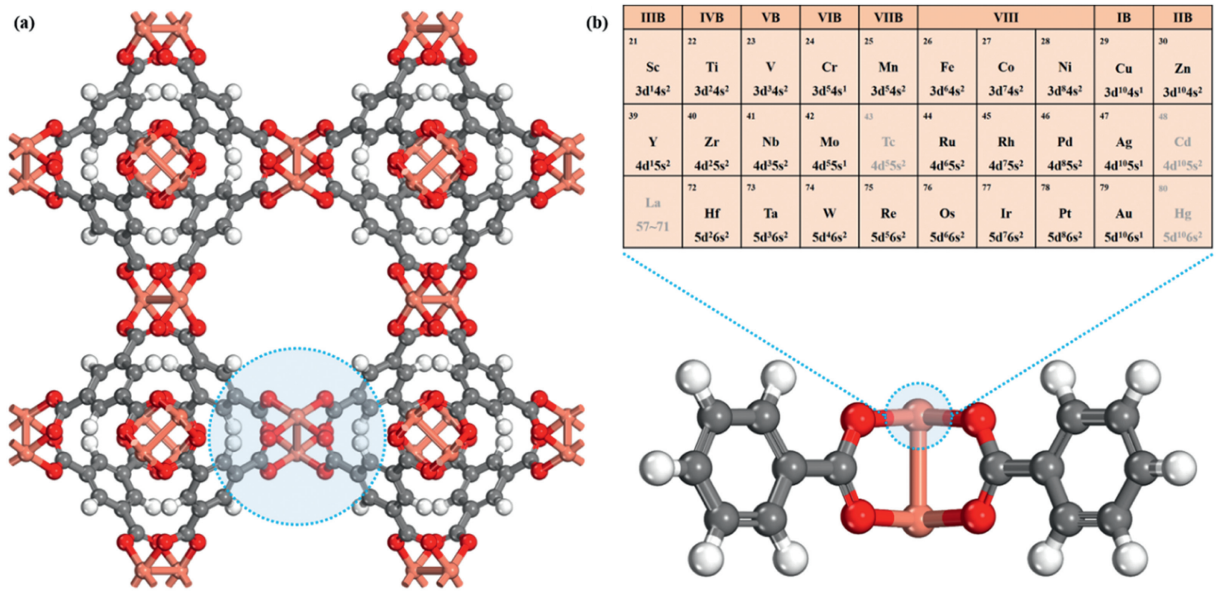

Fig. 1. (a) Unit cell of Cu-BTC, the small cluster truncated for simplified calculation are shown in the blue shadow. (b) The cluster model cut from the unit cell of Cu-BTC, the blue shaded area represents the position of the Cu atom displaced by the TM atom, which is also the metal active site.

Table 1
TM-O bond lengths $d_{TM\text{-}O}$ and the deviation degree ε.

$d_{TM\text{-}O}$ (Å)	Sc	Ti	V	Cr	Mn	Fe	Co	Ni	Cu	Zn
min	2.063	1.978	1.950	2.001	1.924	1.925	1.922	1.888	1.981	2.044
max	2.064	1.978	2.010	2.002	1.924	1.925	1.922	1.888	1.981	2.044
ε/%	0.05	0.00	2.99	0.05	0.00	0.00	0.00	0.00	0.00	0.00
$d_{TM\text{-}O}$ (Å)	Y	Zr	Nb	Mo		Ru	Rh	Pd	Ag	
min	2.214	2.097	2.021	2.096		2.065	2.067	2.058	2.278	
max	2.216	2.098	2.021	2.097		2.065	2.067	2.062	2.279	
ε/%	0.09	0.05	0.00	0.05		0.00	0.00	0.19	0.04	
$d_{TM\text{-}O}$ (Å)		Hf	Ta	W	Re	Os	Ir	Pt	Au	
min		2.070	1.992	2.043	2.042	2.043	2.058	2.053	2.172	
max		2.071	1.992	2.044	2.042	2.043	2.058	2.053	2.173	
ε/%		0.05	0.00	0.05	0.00	0.00	0.00	0.00	0.05	

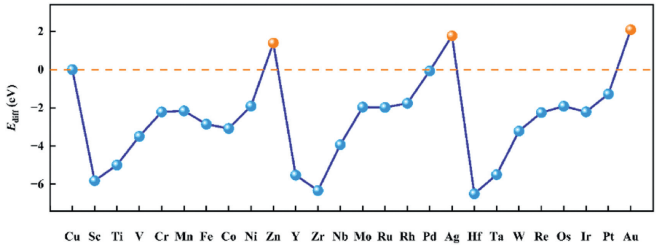

Fig. 2. The substitution energy E_{diff} of CuTM-BTC.

stitution element, CuTM-BTC shows a narrowed HOMO-LUMO gap which still satisfies the POWS redox requirements that LUMO are above reduction potential of H^+/H_2 and HOMO are below the oxidation potential of H_2O/O_2. However, the orbital alignments of rest CuTM-BTCs only satisfy redox potential of half reaction either HER or OER (Fig. S1 in Supporting information). Furthermore, according to the criterion for the adsorption of visible light that 1.6 eV < E_g < 3.2 eV [57,61], the combinations of CuCr-BTC, CuRh-BTC, CuRe-BTC and CuPt-BTC would offer the superior potential to absorb visible light compared with the rest CuTM-BTC.

To investigate the light utilization, the absorption spectra were calculated and are displayed in Figs. 3b and c. It shows that Cu-BTC itself has a strong absorption peak near 525 nm in the visible light region from 390 nm to 780 nm. For 3d-TM substitution, the absorption is blue-shifted and the corresponding absorption peaks for TM of Cr, Fe, Co and Ni appear at 508, 498, 483 and 487 nm, respectively, which fall within the visible light region, among which CuCo-BTC exhibits the strongest absorption peak. Similar tendency is observed for 4d-TM or 5d-TM substitution. The corresponding absorption peaks for TM of Rh, Pd, Re and Pt occur at 531, 496, 480 and 510 nm, respectively. Also, the absorption strengths are increased in compared with the pristine Cu-BTC within the visible light region. Furthermore, CuNi-BTC and CuPt-BTC exhibit the absorption of purple light ranged from 390 nm to 450 nm. Based on the mentioned information, the light absorption capacity of CuTM-BTC is enhanced with respective to the pure Cu-BTC, which promotes the photogeneration of electron-hole pairs.

To further explore light utilization, the distributions of HOMO/LUMO orbitals are described in Fig. 4. HOMO orbitals localized at TM atom are observed for CuTM-BTC with exception of CuRe-BTC, indicating that Cr, Fe, Co, Ni, Rh, Pd or Pt site serves as OER active site due to the photogenerated holes in HOMO. On the other hand, LUMO orbitals at TM atom are found for CuCr-BTC, CuPd-BTC and CuRe-BTC, indicating that Cr, Pd or Re is a HER active site due to the photogenerated electrons in LUMO. Furthermore, we would like to mention that the HOMO/LUMO sep-

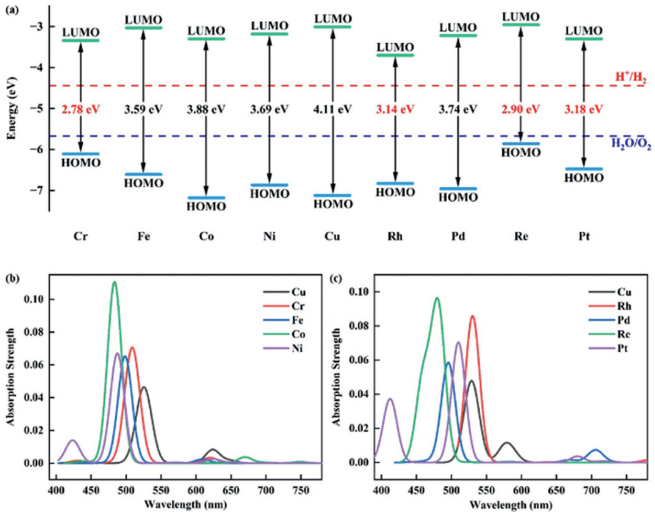

Fig. 3. (a) HOMO-LUMO orbital alignment. (b) Absorption spectrum of CuTM-BTCs wherein TM of 3d-TM of Cr, Fe, Co or Ni. (c) Absorption spectrum of CuTM-BTCs wherein TM of 4d-TM of Rh or Pd, 5d-TM of Re or Pt.

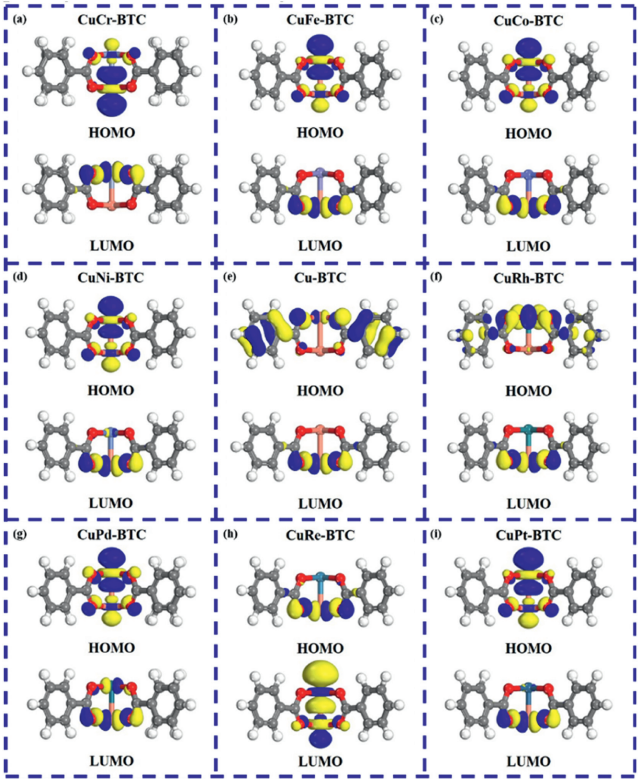

Fig. 4. The distributions of HOMO and LUMO.

aration is only observed at CuRh-BTC, which provides the benefit for suppressing the recombination of photoexcited carriers. However, the HOMO/LUMO overlapping of the rest CuTM-BTCs indicates the photocatalytic activity would suffer from the recombination of photogenerated electrons and photogenerated holes during the reaction.

The Gibbs free energy curves of the two half-reactions, *i.e.*, HER and OER, are shown in Fig. 5. A schematic POWS reaction progress of Cu-BTC has been summarized in Fig. S2 (Supporting information) and the adsorption configurations of the active candidates are provided in Figs. S3-S5 (Supporting information). For HER, ΔG_H is considered as a key descriptor to describe the catalytic activity.

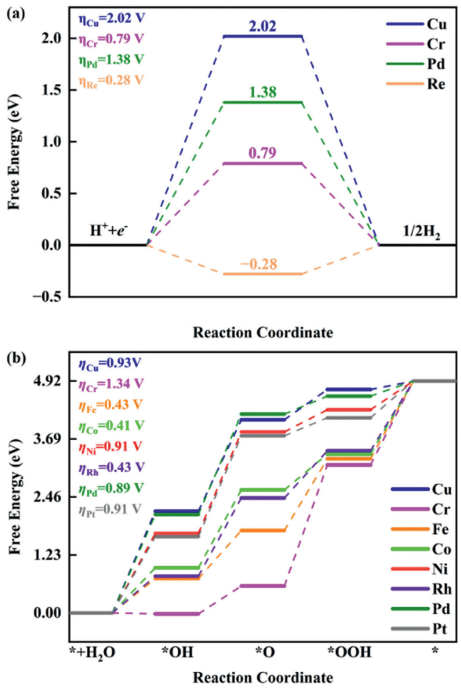

Fig. 5. (a) HER free energy diagrams at the applied potential of 0 V. (b) OER free energy diagrams at the applied potential of 0 V.

According to Sabatier principle [64], the value of ΔG_H for a desirable catalyst should neither be too strong nor too weak in the adsorption of the reactants, that is, the ΔG_H should be zero for an ideal catalyst, achieving the balance between highly efficient proton/electron migration and hydrogen evolution. Fig. 5a presents the Gibbs free energy profiles of HER. As reference, ΔG_H of Cu-BTC is considerably positive with a value of 2.02 eV, suggesting that capturing a proton on Cu-BTC is quite difficult, being super-inert compared to commercial Pt catalyst (−0.09 eV) [65–67]. However, as a Cu atom is substituted by a TM atom, the hydrogen evolution performance is improved wherein the substitution of Cr, Pd, and Re indeed reduce the corresponding thermodynamic barriers. As displayed, the ΔG_H of CuRe-BTC is −0.28 eV, indicating that the adsorption of H on Re site is much stronger than on Cu site, followed by CuCr-BTC (0.79 eV), and CuPd-BTC (1.38 eV). Moreover, from Table S2 and Fig. S6 (Supporting information) that Rh, Co, Pt and Fe sites also have excellent HER performances. However, due to the concentration of their LUMO orbitals at the Cu site, *i.e.*, the concentration of photo-generated electrons, Rh, Co, Pt and Fe sites are not suitable HER active sites.

The OER performance of CuTM-BTC was then investigated. Each stage of the four elementary reactions involved in the entire OER process produces a proton-electron pair. As known, an energy difference of 1.23 eV between two adjacent intermediate states is required for an ideal catalyst, so that OER can occur spontaneously at just above the equilibrium potential. But in reality, there is always a significant difference in the free energy between adjacent steps, which significantly limits the OER process. Fig. 5b shows the free energy profiles of CuTM-BTC. From the diagram, there is a free energy barrier observed for Cu-BTC with η^{OER} of 0.93 V, which has no advantage in competition with benchmark IrO_2 with overpotential of 0.56 V [68]. From Table S2 and Fig. S7 (Supporting information), the potential-determining step (PDS) is *O formation for CuCo-BTC, CuNi-BTC, CuRh-BTC, CuPd-BTC, and CuPt-BTC, and the corresponding η^{OER} are 0.41 V, 0.91 V, 0.43 V, 0.89 V, and 0.91 V, respectively; PDS for CuFe-BTC is OOH* deprotonation, with a low η^{OER} of 0.43 V; PDS of *OOH formation for CuCr-BTC causes a high

Table 2
HOMO-oxidation offset (HOO), LUMO-reduction offset (LRO), and HER/OER overpotentials.

Parameter	Cr	Fe	Co	Ni	Cu	Rh	Pd	Re	Pt
LRO (eV)	1.10	1.41	1.14	1.26	1.43	0.74	1.22	1.48	1.14
η^{HER} (V)	0.79	0.76	0.42	1.88	2.02	0.01	1.38	0.28	0.44
HOO (eV)	0.44	0.94	1.51	1.20	1.45	1.16	1.29	0.19	0.81
η^{OER} (V)	1.34	0.43	0.41	0.91	0.93	0.43	0.89	1.94	0.91

overpotential of 1.34 V. Herein, CuFe-BTC, CuCo-BTC and CuRh-BTC are even superior to IrO_2 catalyst [68], indicating their enormous potentiality for OER.

The thermodynamic feasibility of a photo-redox reaction can be assessed by the HOMO-oxidation offset (HOO) and the LUMO-reduction offset (LRO) [57]. The HOO is taken to be the difference between HOMO of CuTM-BTC and the oxidation potential of H_2O/O_2. And LRO is associated with the reduction potential of H^+/H_2, defined as the difference between LUMO and the reduction potential of H^+/H_2. Table 2 lists the LRO, HOO, and HER/OER overpotentials to assess the driving force that CuTM-BTC can provide. In order to boost photocatalysis, it should be that LRO $\geq \eta^{HER}$ and HOO $\geq \eta^{OER}$. For pristine Cu-BTC, its LRO is inadequate to get over the large HER overpotential (1.43 eV *vs.* 2.02 V), indicating that it is not suitable to reduce H^+ to H_2. Yet this is not the case for OER side, because Cu-BTC has a sufficiently large HOO to overcome its OER overpotential (1.45 eV *vs.* 0.93 V). Therefore, the POWS rate of Cu-BTC suffers from the sluggish HER activity. For CuTM-BTC, CuCr-BTC and CuRe-BTC are excellent HER photocatalysts wherein the corresponding LRO are 1.11 eV and 1.48 eV and η^{HER} are 0.79 V and 0.28 V, respectively. However, CuPd-BTC is unable to boost HER owing to LRO of 1.22 eV less than η^{HER} of 1.38 V. On the other hand, CuFe-BTC, CuCo-BTC, CuNi-BTC, CuRh-BTC and CuPd-BTC do have sufficient driving force to boost OER and are capable to oxidize H_2O into O_2, among which CuFe-BTC, CuCo-BTC, and CuRh-BTC are promising due to the low η^{OER} less than 0.5 V. Therefore, based on mentioned discussions, it recommends that using Cr or Re as substitution element to boost HER photocatalysis and using Fe, Co or Rh as substitution element to boost OER photocatalysis.

Herein, before closing the activity discussions, we also considered the reactivity of Cu sites in CuTM-BTC and the corresponding overpotentials are listed in Table S3 (Supporting information). For HER side, η^{HER} of Cu sites are remarkably higher than those of Cr site and Re site for CuCr-BTC and CuRe-BTC, respectively indicating its infeasibility to boost HER; for OER side, in despite of the reduced η^{OER} of Cu sites with the values around 0.9–1.0 V, Cu is still inactive since η^{OER} are still higher than the corresponding thermodynamic driving forces wherein HOO are 0.44 eV for CuCr-BTC and 0.19 eV for CuRe-BTC, respectively. In the sense, CuCr-BTC and CuRe-BTC are functional toward HER catalyzed by TM sites. Similarly, Cu sites of CuFe-BTC, CuCo-BTC, and CuRh-BTC are inactive due to the high η ($\eta^{HER} \geq 1.5$ V and $\eta^{OER} \geq 1.0$ V).

Last but not least, we would like to mention that our proposed candidates are expected to be synthesized based on the following information. Xia *et al.* [69] found that replacing Cu metal nodes in Cu-BTC with trace amounts of Ru (0.44 wt%) not only enhances its stability in aqueous solutions, but also increases the photocatalytic hydrogen production efficiency by 50%. Interestingly, our results are consistent with the work of Xia *et al.* [69]. From Table S1 and Fig. S8 (Supporting information), the LUMO of CuRu-BTC is −3.68 V and the η^{HER} is 0.01 V which reflects its good HER activity; however, the HOMO of CuRu-BTC is above the oxidation potential of H_2O/O_2, demonstrating that Ru is not a suitable active site, which is also proved by the large η^{OER} with the value of 0.84 V. Furthermore, using one-step hydrothermal synthesis method, Hu *et al.* [70] fabricated a bimetallic porous structure Ni/Cu-BTC with a regular octahedral structure similar to Cu-BTC and found the bimetallic structure has good dye adsorption capacity. Similarly, Cu/Co-BTC, a bimetallic-organic porous material with a paddle-wheel structure, had been successfully assembled by Tian *et al.* [71] with a solvothermal approach and the results showed that the bimetallic structure improved the desulfurization performance by 30%. Similarly, Wang *et al.* [72] synthesized bimetallic Zn/Cu-BTC *via* replacing Cu in Cu-BTC with Zn in the desulfurization application. Therefore, the strategy of partially replacing metal nodes is feasible in experiments. Furthermore, to support the synthesis of the candidates we figured out, the formation energies E_{form} of CuCr-BTC, CuRe-BTC, CuFe-BTC, CuCo-BTC, and CuRh-BTC are evaluated and listed in Table S4 (Supporting information). E_{form} of CuTM-BTC are all negative and the values are in the range from −0.30 eV to −0.24 eV, which is comparable to the value of pure Cu-BTC. Therefore, the formation of the mentioned CuTM-BTC is energetically possible. In the regard, it is reasonable to expect the experimental verification of our proposed candidates.

In this study, density functional theory calculations have been used to systematically explore the feasibility of Cu-BTC and its derivatives as POWS materials. The structural and photoelectric properties of pristine Cu-BTC indicate that it is not a suitable for POWS, because of a wide HOMO-LUMO gap with the value of 4.11 eV, combined with a large overpotential for HER and OER with a value of 2.02 V and 0.93 V. Fully considering the frontier orbital distributions and the thermodynamic barriers of CuTM-BTC, Cr and Re can serve as active sites for HER and the corresponding η^{HER} are 0.79 V and 0.28 V, and CuFe-BTC, CuCo-BTC and CuRh-BTC are capable to catalyze OER due to their low η^{OER} that less than 0.5 V. Therefore, our work provides a vivid strategy for developing a high-effective Cu-BTC derivative in the application of overall water splitting.

Declaration of competing interest

The authors declare that they have no known competing financial interests or personal relationships that could have appeared to influence the work reported in this paper.

Acknowledgments

The authors greatly acknowledge the financial support from National Natural Science Foundation of China (No. 21503097), Postgraduate Research & Practice Innovation Program of Jiangsu Province (No. KYCX23_3905).

Supplementary materials

Supplementary material associated with this article can be found, in the online version, at doi:10.1016/j.cclet.2024.109720.

References

[1] J.Y. Liu, S.M. Zhu, B. Wang, et al., Chin. Chem. Lett. 34 (2023) 107749.
[2] Y.B. Wu, C. He, W.X. Zhang, J. Energy Chem. 82 (2023) 375–386.
[3] X.Y. Liu, C.G. Jia, G.M. Jiang, et al., Chin. Chem. Lett. 35 (2024) 109455.
[4] M.G. Kibria, H.P.T. Nguyen, K. Cui, et al., ACS Nano 7 (2013) 7886–7893.
[5] Y. Liu, X.W. Zhang, L.S. Lu, et al., Chin. Chem. Lett. 33 (2022) 1271–1274.
[6] W.X. Zhang, S. Xi, Y. Liang, C. He, Appl. Surf. Sci. 608 (2023) 155106.
[7] A. Fujishima, K. Honda, Nature 238 (1972) 37–38.
[8] Q. Wang, K. Domen, Chem. Rev. 120 (2020) 919–985.
[9] J. Suntivich, K.J. May, H.A. Gasteiger, J.B. Goodenough, Science 334 (2011) 1383–1385.
[10] Q. Guo, C.Y. Zhou, Z.B. Ma, X.M. Yang, Adv. Mater. 31 (2019) 1901997.
[11] K. Maeda, K. Domen, J. Phys. Chem. C 111 (2007) 7851–7861.
[12] A. Kudo, Y. Miseki, Chem. Soc. Rev. 38 (2009) 253–278.
[13] H. Kato, K. Asakura, A. Kudo, J. Am. Chem. Soc. 125 (2003) 3082–3089.
[14] P. Peerakiatkhajohn, J.H. Yun, H.J. Chen, et al., Adv. Mater. 28 (2016) 6405–6410.
[15] F. Boudoire, R. Toth, J. Heier, et al., Energy Environ. Sci. 7 (2014) 2680–2688.
[16] T. Heine, Acc. Chem. Res. 48 (2015) 65–72.

[17] Q.H. Wang, K. Kalantar-Zadeh, A. Kis, et al., Nat. Nanotechnol. 7 (2012) 699–712.
[18] K. Li, M. Han, R. Chen, et al., Adv. Mater. 28 (2016) 8906–8911.
[19] J.G. Hou, H.J. Cheng, O. Takeda, H.M. Zhu, Energy Environ. Sci. 8 (2015) 1348–1357.
[20] C. He, J.L. Ma, Y.B. Wu, W.X. Zhang, J. Energy Chem. 84 (2023) 131–139.
[21] M.J. Liao, J.Y. Feng, W.J. Luo, et al., Adv. Funct. Mater. 22 (2012) 3066–3074.
[22] W.J. Ong, L.L. Tan, Y.H. Ng, et al., Chem. Rev. 116 (2016) 7159–7329.
[23] X.C. Wang, K. Maeda, A. Thomas, et al., Nat. Mater. 8 (2009) 76–80.
[24] Y. Zheng, J. Liu, J. Liang, et al., Energy Environ. Sci. 5 (2012) 6717.
[25] Y. Zhang, L.T. Wu, S.P. Wang, et al., Chin. Chem. Lett. 35 (2024) 108551.
[26] K. Maeda, K. Teramura, N. Saito, et al., J. Catal. 243 (2006) 303–308.
[27] A. Sinhamahapatra, J.P. Jeon, J.S. Yu, Energy Environ. Sci. 8 (2015) 3539–3544.
[28] Y. Yuan, J.N. Pan, W.N. Yin, et al., Chin. Chem. Lett. 35 (2024) 108724.
[29] Y.J. Lin, Y. Xu, M.T. Mayer, et al., J. Am. Chem. Soc. 134 (2012) 5508–5511.
[30] C.D. Lv, G. Chen, X. Zhou, et al., ACS Appl. Mater. Interfaces 9 (2017) 23748–23755.
[31] F. Yu, L.C. Wang, Q.J. Xing, et al., Chin. Chem. Lett. 31 (2020) 1648–1653.
[32] A. Naseri, M. Samadi, A. Pourjavadi, et al., J. Mater. Chem. A 5 (2017) 23406–23433.
[33] J.W. Fu, J.G. Yu, C.J. Jiang, B. Cheng, Adv. Energy Mater. 8 (2018) 1701503.
[34] S.W. Cao, J.G. Yu, J. Phys. Chem. Lett. 5 (2014) 2101–2107.
[35] J.J. Wang, Z.Y. Guan, J. Huang, et al., J. Mater. Chem. A 2 (2014) 7960–7966.
[36] L.N. Wang, Z.J. Liu, J.M. Zhang, et al., Chin. Chem. Lett. 34 (2023) 108007.
[37] T.L. Xia, Y.C. Lin, W.Z. Li, M.T. Ju, Chin. Chem. Lett. 32 (2021) 2975–2984.
[38] P. Horcajada, C. Serre, G. Maurin, et al., J. Am. Chem. Soc. 130 (2008) 6774–6780.
[39] J.S. Seo, D. Whang, H. Lee, et al., Nature 404 (2000) 982–986.
[40] S. Horike, M. Dincă, K. Tamaki, J.R. Long, J. Am. Chem. Soc. 130 (2008) 5854–5855.
[41] W.G. Zeng, Y.C. Dong, X.Y. Ye, et al., Chin. Chem. Lett. 35 (2024) 109252.
[42] J.R. Li, R.J. Kuppler, H.C. Zhou, Chem. Soc. Rev. 38 (2009) 1477.
[43] W.F. Zhang, L. Wang, G.C. Ding, et al., Chin. Chem. Lett. 34 (2023) 107328.
[44] W.X. Zhang, Z. Li, J.H. Zhang, et al., J. Alloy. Compd. 971 (2024) 172669.
[45] H.B. Qiu, Y. Inoue, S.N. Che, Angew. Chem. Int. Ed. 48 (2009) 3069–3072.
[46] S.S.Y. Chui, S.M.F. Lo, J.P.H. Charmant, et al., Science 283 (1999) 1148–1150.
[47] K. Schlichte, T. Kratzke, S. Kaskel, Micropor. Mesopor. Mat. 73 (2004) 81–88.
[48] X.Q. Dong, X.Y. Liu, Y.F. Chen, M.H. Zhang, J. CO_2 Util. 24 (2018) 64–72.
[49] M. Jin, X.F. Qian, J.K. Gao, et al., Inorg. Chem. 58 (2019) 8332–8338.
[50] F.A. Sofi, K. Majid, O. Mehraj, J. Alloy. Compd. 737 (2018) 798–808.
[51] S.S. Xu, H.L. Huang, X.Y. Guo, et al., Sep. Purif. Technol. 257 (2021) 117979.
[52] Z.W. Liu, K. Zhang, Y. Wu, H.X. Xi, J. Mater. Sci. 53 (2018) 6080–6093.
[53] J.Y. Ye, C.J. Liu, Chem. Commun. 47 (2011) 2167.
[54] S. Ketrat, T. Maihom, S. Wannakao, et al., Inorg. Chem. 56 (2017) 14005–14012.
[55] Y. Wang, J.F. Yang, Z.J. Li, et al., RSC Adv. 5 (2015) 33432–33437.
[56] X. Chen, Y.H. Li, M.X. Leng, Colloid Surf. A 644 (2022) 128882.
[57] B. Mourino, K.M. Jablonka, A. Ortega-Guerrero, B. Smit, Adv. Funct. Mater. 33 (2023) 2301594.
[58] J.K. Xu, Q. Wan, M. Anpo, S. Lin, J. Phys. Chem. C 124 (2020) 6624–6633.
[59] M. Idrees, B. Amin, Y. Chen, X. Yan, Appl. Surf. Sci. 615 (2023) 156260.
[60] H. Zhu, X. Zhang, Y. Nie, et al., Appl. Surf. Sci. 635 (2023) 157694.
[61] W.Y. Zhou, L.C. Dong, L.X. Tan, Q. Tang, J. Phys. Chem. C 125 (2021) 7581–7589.
[62] T. Das, G. Di Liberto, S. Tosoni, G. Pacchioni, J. Chem. Theory Comput. 15 (2019) 6294–6312.
[63] I. Singh, A.A. El-Emam, S.K. Pathak, et al., Mol. Simulat. 45 (2019) 1029–1043.
[64] M.C. Zhang, K.X. Zhang, X. Ai, et al., Chin. J. Catal. 43 (2022) 2987–3018.
[65] P. Sen, K. Alam, T. Das, et al., J. Phys. Chem. Lett. 11 (2020) 3192–3197.
[66] J. Li, J. Zhang, J. Zhang, et al., J. Mater. Chem. A 11 (2023) 19812–19844.
[67] J. Li, N.T. Wu, J. Zhang, et al., Nano Micro Lett. 15 (2023) 227.
[68] I.C. Man, H.Y. Su, F. Calle-Vallejo, et al., ChemCatChem 3 (2011) 1159–1165.
[69] J.H. Xia, X.Y. Liu, H.B. Zhou, et al., Catal. Sci. Technol. 11 (2021) 7905–7913.
[70] J. Hu, H.J. Yu, W. Dai, et al., RSC Adv. 4 (2014) 35124–35130.
[71] F.P. Tian, C.X. Qiao, R.Y. Zheng, et al., RSC Adv. 9 (2019) 15642–15647.
[72] T.T. Wang, X.X. Li, W. Dai, et al., J. Mater. Chem. A 3 (2015) 21044–21050.